

Fabrication of Flexible Cu–TiO₂ Nanosheet Photocatalysts on Carbon Cloth for Solar Hydrogen Production via a Self-Healing Cu Redox Loop

Mariyum Yousaf¹, Phommachanh Anny¹, Hui Hu¹, Muhammad Sohail^{*2}, Yun Gao^{*1}

¹Ministry of Education Key Laboratory for the Green Preparation and Application of Functional Materials, School of Materials Science & Engineering, Hubei University, Wuhan, Hubei 430062, People's Republic of China.

²Department of Natural Sciences, Faculty of Science and Engineering, Manchester Metropolitan University, Manchester M15 6BX, United Kingdom

Corresponding Authors: Email: gaoyun@hubu.edu.cn, mohammad.sohail@mmu.ac.uk

Contents:	1
Experimental Details.....	2
Materials.....	2
Synthesis of Catalyst.....	2
Characterization of Synthesized Catalyst.....	3
Methanol steam Reforming test for hydrogen production.....	4
Photocatalyst weight calculation.....	5
Apparent Quantum Yield.....	5
Figure S1. XRD/Raman spectra of pristine TNS@CC and Cu decorated CC.....	5
Figure S2. SEM images of bare Carbon	6
Figure S3. SEM and EDS spectra of 7%Cu-TNS@CC.....	7
Figure S4. SEM and EDS spectra of 12%Cu-TNS@CC.....	8
Figure S5. UV-Vis- Analysis.....	9
Figure S6. TRPL Graph of 9wt%-12wt% CuTNS@CC.....	9
Table S1. TRPL(ns).....	10
Table S2. The de-convoluted binding energies from Cu 2p _{3/2} and the corresponding atomic percentage.....	10
Figure S7. Graphical representation of 10%Cu-TNS@CC test.....	11
Table S3: H ₂ evolution rate of Cu-TiO ₂ using carbon cloth as a substrate.....	11
Figure S8: N ₂ adsorption-desorption isotherm.....	12
Table S4: BET surface analysis and pore size distribution.....	12
Figure S9. Figure: UPS spectrum analysis	12

Figure S10. Figure: LSV and CV spectrum analysis	13
Figure S11. Figure: Multiple cycles of cyclic voltammetry.....	13
Electrocatalytic HER Performance of Cu-TNS@CC (Discussion).....	14

Experimental Details

Material

All chemicals used in this work were of analytical grade and used without any further purification. Typically, the chemicals include acetone (SCR Shanghai Test China), Ethanol and Methanol CH₄O (SCR Shanghai Test China), DI water (18.25 MΩ), TiCl₃ (Aladdin Industrial Co., Shanghai, China), hydrochloric acid (HCl, 37%, Tianjin Chemicals), CuCl₂·2H₂O (SCR-shanghai china), Titanium butoxide (>99.0% Aladdin Industrial Co., Shanghai, China), hydrofluoric acid (HF AR,>40%, (SCR-Shanghai China), conductive Carbon cloth (SCI-Material Hub), Ultra-pure water.

Synthesis

Cleaning carbon cloth (CC): Carbon cloth (substrate) was ultrasonically washed with acetone, DI-water, and ethanol sequentially, then dried at 80 °C for 90min.

TiO₂ coated seed layer CC (TNS@CC): Cleaned CC (3 x 3 cm), was immersed in a mixture solution of HCl(1ml) and ultrapure water (60ml), and 1ml TiCl₃ (is drop-wise added into the mixture solution to get transparent solution), treated in an oven at 80 °C for 90 minutes. Washed with ethanol and dried (80 °C), then annealed at 500 °C for 120 minutes.

%Cu- TNS@CC (0.5-12Wt%) nanosheet was prepared by adding the 5ml of Titanium Butoxide [Ti (OBU)₄] slowly dropwise into 30ml mixture solutions of hydrochloric acid (HCl) and DI H₂O with volume ratio of 1:1 in the presence of Hydrofluoric acid (1ml) followed by 0.5-12 %(CuCl₂·3H₂O), stirred for two hrs. until clear solution formed. Transferred this clear solution to a Teflon-lined stainless steel autoclave with a capacity of 100 mL, along with a TiO₂ seed layer coated CC at a certain angle against the wall of the autoclave and thermally treated at 160 °C for 960 minutes. When the oven cools down to room temperature naturally, %Cu-TiO₂NS@CC samples removed and washed with DI-water and EtOH 3-times and dried at 60C for 4h. Identically, Cu-TNS@CC samples with different %Cu weight concentrations ranging from 0.5 to 12wt % were prepared to optimize HER and assigned as x%Cu-TNS@CC (TNS = TiO₂ nanosheet at carbon cloth x=0.5-12). For comparison, bare TiO₂ (TNS@CC) were prepared similarly without the addition of the Cu precursor. The optimized 10% Cu-TNS@CC with HER rate of 1765 μmolg⁻¹h⁻¹ was reproduced. The 10% Cu-TNS@CC was reproduced with an average HER rate of 1745 μmolg⁻¹h⁻¹.

Instrumentations of the synthesized catalyst

The prepared photocatalyst analyzed by different characterization techniques. Phase structures of catalyst were examined by (Bruker, D8 Advance) X-ray diffraction. X-ray diffraction (XRD) patterns were captured at 40kV and 40mA via Cu-K α radiation source ($K\alpha = 1.54056 \text{ \AA}$) time 0.1s per dot. The morphology and crystal size of the (Cu-TiO₂) photocatalyst were analyzed by Field Emissions Scanning Electron Microscopy (FESEM) Sigma 500, Zeiss, 15kv, 30um. Using a UV-Vis spectrometer (UV-3600, Shimadzu, Japan), air as baseline, slit width 5mm, external dual detector, scanning speed medium one point every 0.5 nm. UPS (band edges) analysis carried out by instrumental model "Thermo SCIENTIFIC ESCALAB 250Xi, using high-intensity UV lamp utilizing HeI (21.22 eV) for valence band analysis. The X-ray photo-electron spectroscopy used to study the chemical valence state of Cu doped TiO₂ photocatalyst Instrument Model: Thermo SCIENTIFIC ESCALAB 250Xi X-ray Photoelectron Spectrometer (XPS); X-Ray source of radiation: Al Ka source, X-ray energy 1486.6eV, energy resolution better than 0.45eV Tested light spot area of 500 microns, electronic neutralizing gun for charge compensation X-ray tube voltage 15kv, current 10mA, Analytical chamber background vacuum 10⁻⁹ mbar. Photoluminescence (PL) emission spectra Fluo time300,PICOQUANTExc_Bandpass 1.5 nm, Exc Polarization 0.0°, Exc Source PDL 820, Exc Filter 1, Exc Intensity 90 %, Exc Attenuation open (5), Det Band pass 2.7nm, Depolarization, Det Lens Position 7.3mm, Det Attenuation 100 %, Det Filter 400 (4) Det Grating 1200gr 500bl (1), Detector UV-red [PMT], Mean Time 0.1 s, Meas Bin Width 200 ps, Meas Base Resolution 25 ps, Sync Frequency 40000000 , Sync Source PDL 820, Photon Counter Time Harp 260 P 1034100 0121-0422-02.0, Easy Tau 3293, Signal CFD Level -28 mV , Signal CFD Zero Cross -10 mV , Signal Offset -18000 ps, Signal Enable true, Sync CFD Level -150 mV, Sync CFD Zero Cross -10 mV , Sync Offset 0 ps, Sync Div. 8, and Raman spectra (Thermo Scientific DXR3). Surface area and porosity (measured by Micrometrics ASAP 2020 Plus) of the synthesized catalyst were evaluated using N₂ adsorption-desorption measurements. Analysis adsorptive: N2 Analysis bath temp -195.800 °C Thermal correction Yes, Sample mass 0.1225 g, Ambient free space 26.7648 cm³ Measured Analysis free space 79.5467 cm³ Equilibration interval 20 s Low pressure dose 8.0000 cm³/g STP Sample density 1.000 g/cm³.

Methanol steam Reforming test for hydrogen production

A methanol steam reforming test was carried out at room temperature. An air-tight quartz reactor with a capacity of 200ml was used; the inlet and outlet of the quartz reactor were sealed with silicone rubber sockets to stop product leakage. 10%Cu-TNS@CC (3 x 3 cm) placed horizontally in 100ml water (80ml) methanol (20ml) solution (1:4). Before being exposed to light irradiation, the reaction system purged to high purity N₂ flow for 20 minutes to ensure air free space in the quartz reactor, also breakdown the oxygen inside the quartz reactor, making the inactive environment inside the reactor. Photoreforming catalytic reaction was carried out under an Xe arc lamp; a focused Xe arc lamp (Au Light, China) was utilized to illuminate the reactor during photocatalytic processes. The reaction product is collected after one hour (H₂ gas) and evaluated using an off-line gas chromatograph machine (GC-2018, Shimadzu, Japan) equipped with a thermal conductivity detector (TCD) and a molecular sieve 5A column, with N₂ as the carrier gas. For recyclability and reproducibility of the sample (10%Cu-TNS@CC), the produced gas (H₂) was removed from the quartz reactor at regular intervals (5h) and refilled with N₂ for the next cycle (10 minutes). The H₂ evolution process was repeated for 20 hours (4 cycles). The H₂ production maintenance ratio is 96% after four cycles (20 h), revealing an excellent catalytic cycling strength and a highly photo-corrosion resistant.

Photocatalyst Weight Calculation

Weight of Catalyst at Substrate = catalyst net weight (mg) -weight of Substrate(mg)

Apparent Quantum Yield

The apparent quantum efficiency (AQY) of 10%Cu is calculated via the following formula:

$$AQY(\%) = Ne/Np$$

Ne is the total number of electrons transferred during reactions, Np is the number of incident photons, and n represents the number of evolved hydrogen molecules. The calculation formulas are given as:

$$Ne = 2 \times n,$$

$$Np = IA\lambda \cdot \frac{t}{hc}$$

Where I is the incident photons, A is the incident light area, t is the reaction time, λ represents the incident light wavelength, h is Planck's constant, and c is the speed of light. The average power of UV light

(416 + 10nm) is $52.76\text{mW}/\text{cm}^2$, which was identified by a photo-radiometer (PL – MW 2000, Perfect Light). The highest hydrogen production rate of 0.62mmol in two hours for the 10%Cu was used to calculate t , so the value of Ne was estimated to be 7.467×10^{20} . The diameter of the photocatalytic reactor is 3.3cm , so the value of A should be 8.5cm^2 , the reaction time t is 3600sec , and the AQE of 10%Cu irradiated by 416nm light is by substituting the above value into the given formula. AQE at 416nm is 18.71%. Calculation steps are as follows

$$AQE(\%) = (Ne/Np)100\%$$

$$AQE(\%) = (7.467 \times 10^{20} / 3.399 \times 10^{21})100\%$$

$$AQE(\%) = 18.71\%.$$

Now for the same set of values ($I = 52.76 \times 10^{-3}\text{W}/\text{cm}^2$, $A = 23.5\text{cm}^2$, $t = 3600\text{sec}$) except when the highest H_2 production rate of 0.673mmol in 2 hours is used. Then $Ne = 8.103 \times 10^{20}$ and at 450nm the corresponding AQE is 22.02%.

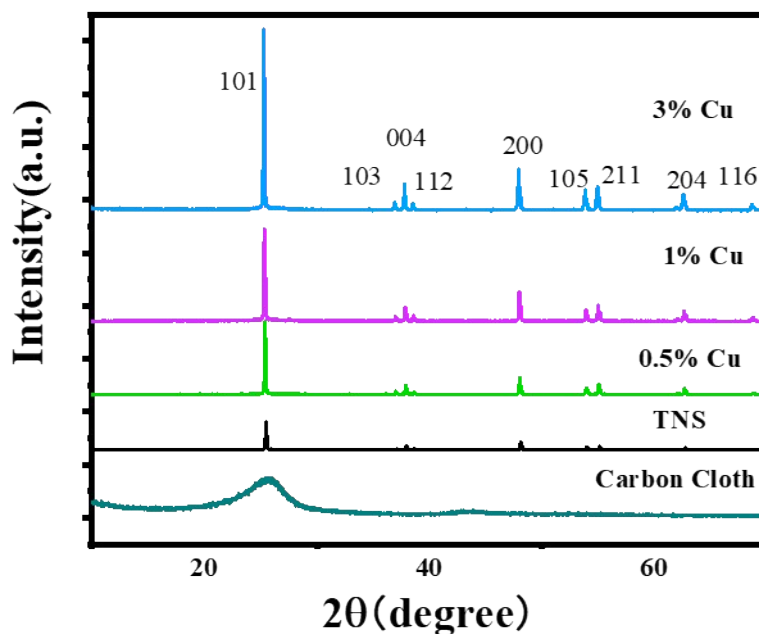


Figure S1: XRD spectra of pristine TNS@CC and low Cu concentration decorated TNS@CC.

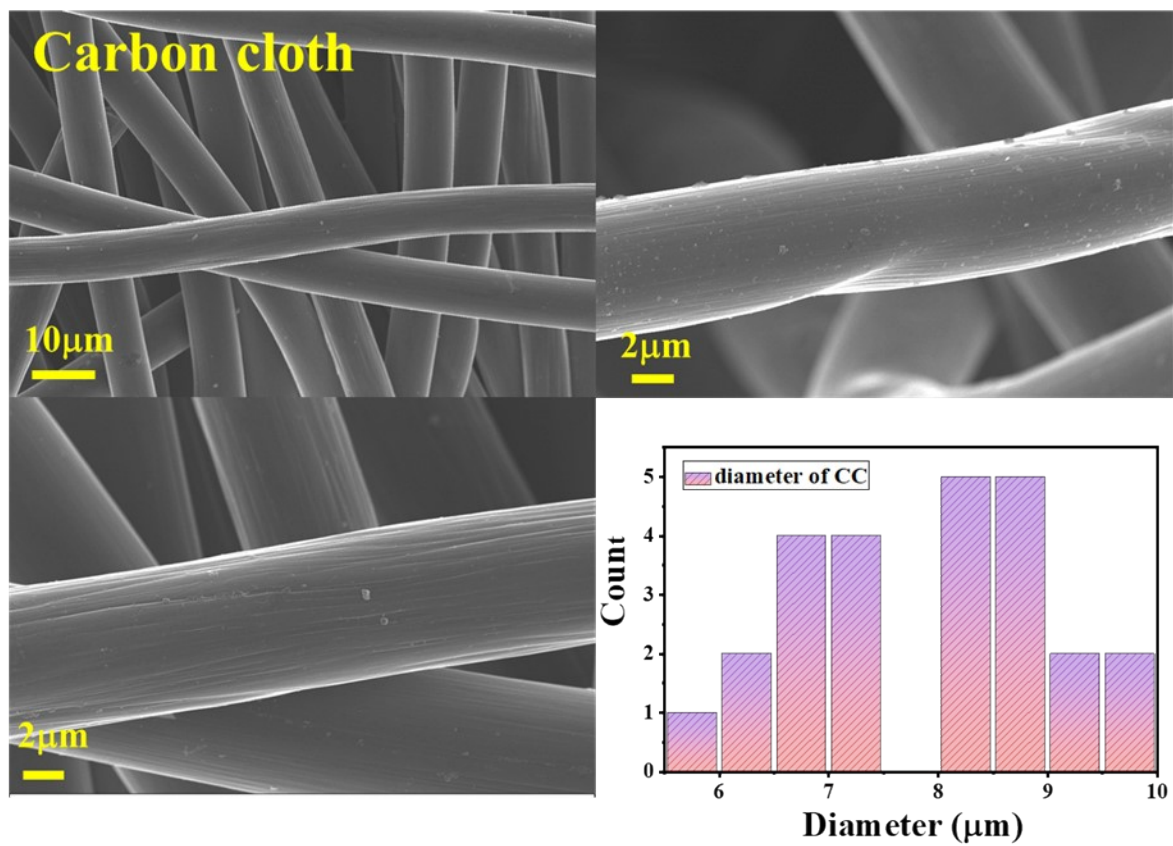


Figure S2: SEM images of bare carbon cloth (CC) at different resolution , with average diameter of bare carbon cloth.

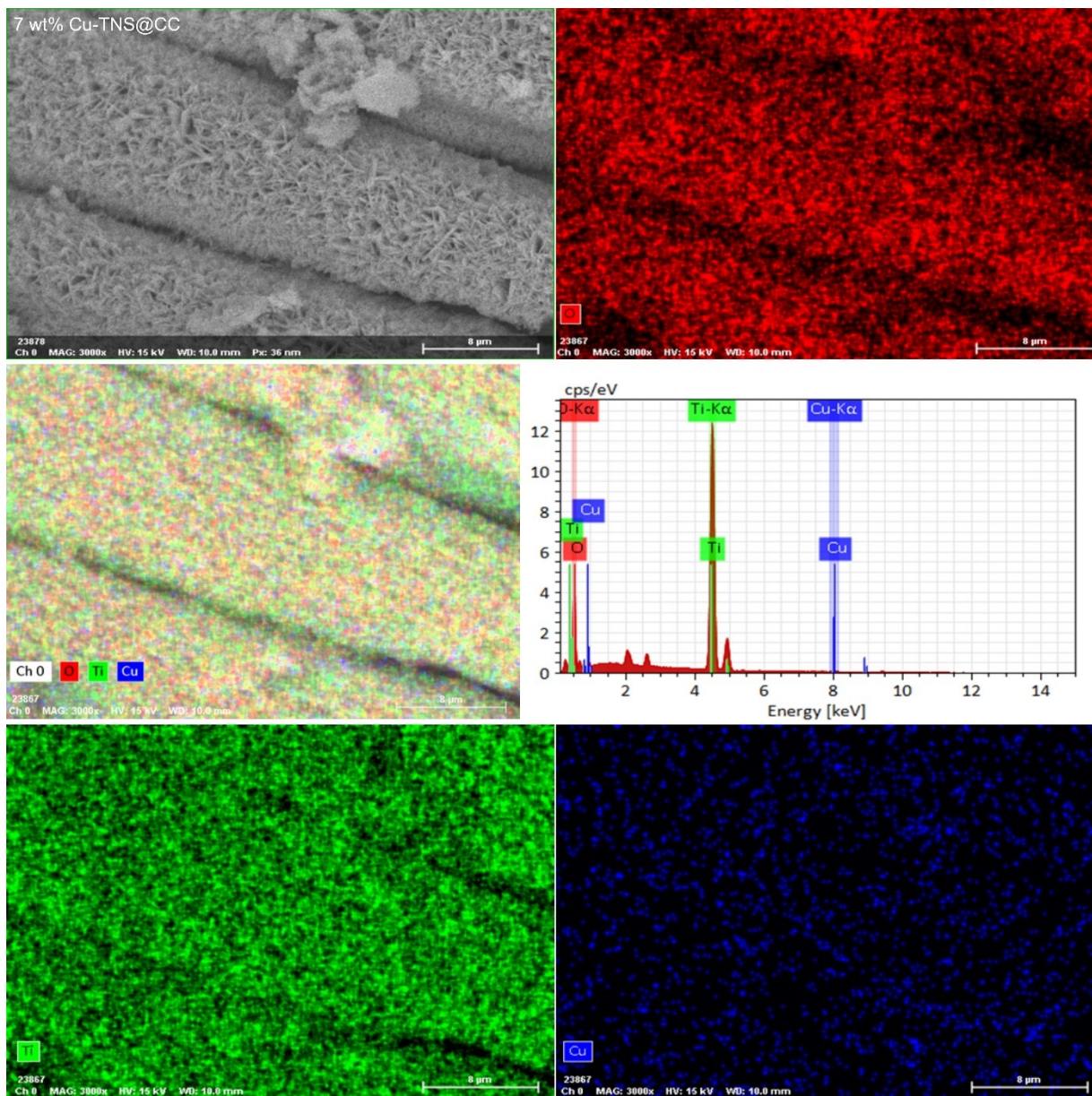


Figure S3: SEM and EDS spectra of 7%Cu-TNS@CC.

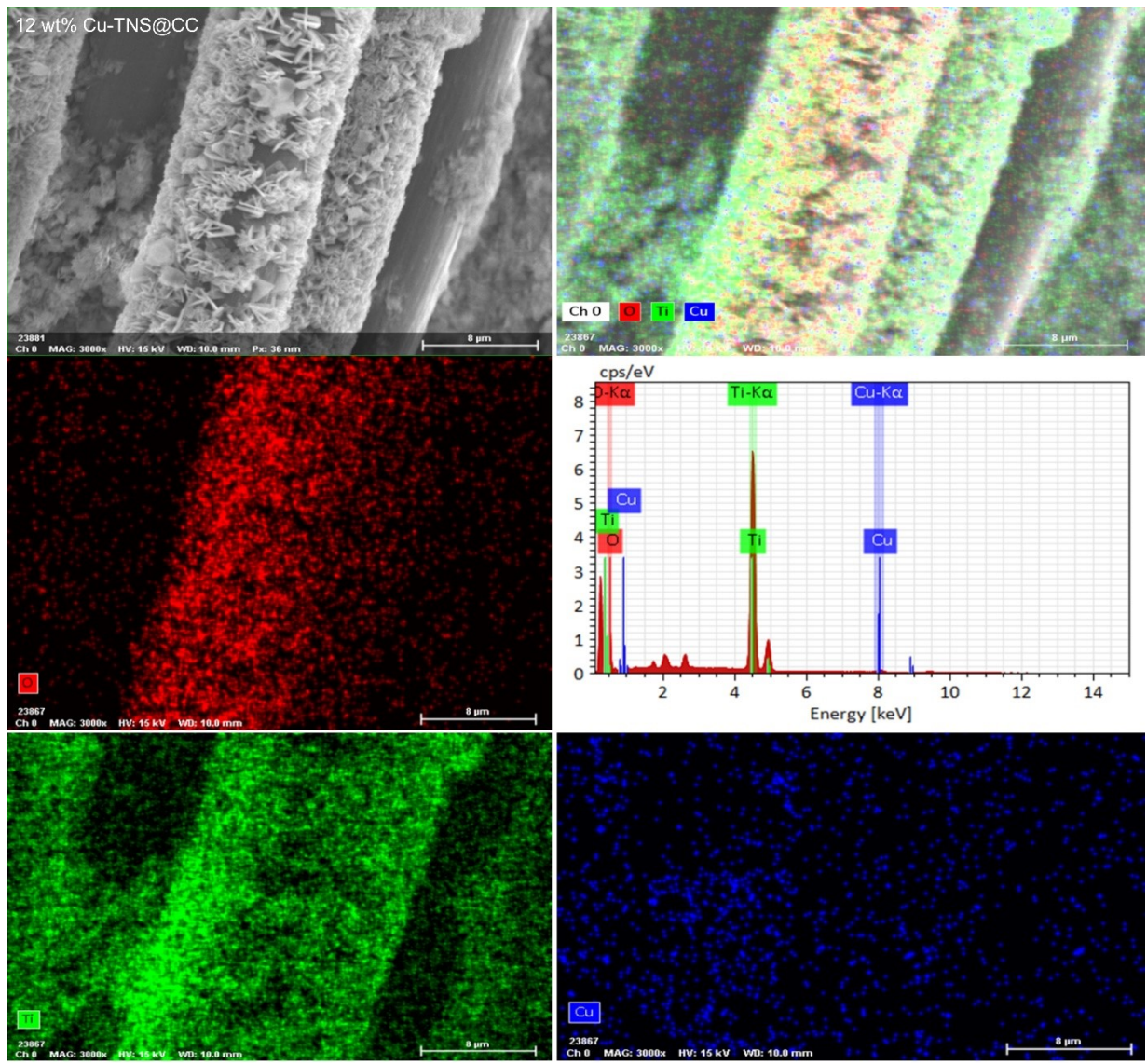


Figure S4: EDS mapping of 12% Cu-TNS@CC.

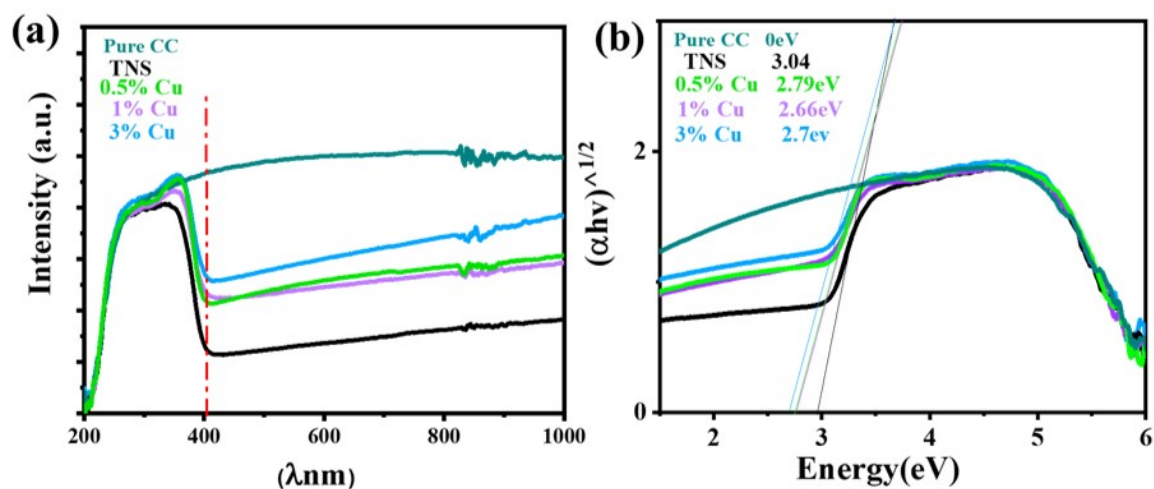


Figure S5: (a) UV-absorption spectra of %Cu and TNS, Pristine TiO₂ and plan carbon cloth, (b) TAUC plot of %Cu and TNS, Pristine TiO₂ and plan carbon cloth.

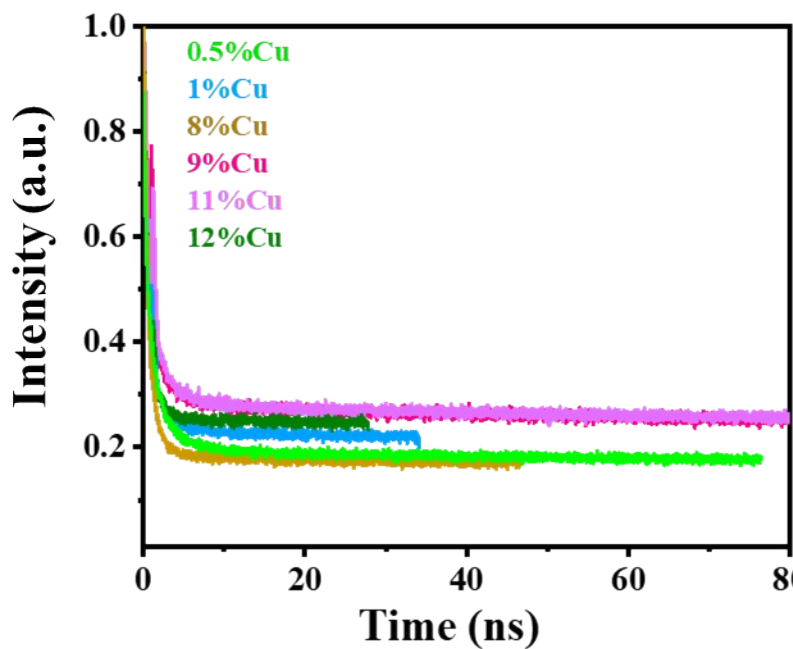


Figure S6: TRPL spectra of varying %Cu-TNS@CC.

Table S1: Time decay of different wt% Cu-TNS@CC

Prepared nanosheets	Time decay(ns)
0.5%Cu	9.43
1%Cu	7.9
8%Cu	12
9%Cu	6.5
11%Cu	6.1
12%Cu	8

Table S2. The de-convoluted binding energies from Cu 2p_{3/2} and the corresponding atomic percentage

Catalyst	Cu 2p _{3/2} (Cu ⁰) Binding-energy (eV)	Atomic (%)	Cu 2p _{3/2} (Cu ₂ O) Binding- energy (eV)	Atomic (%)	Cu2p _{3/2} (CuO) Binding-energy (eV)	Atomic (%)
10%Cu	931.2 eV	13.54	932.5 eV	26.52	934.96 eV	59.94
10%Cu Recycled	931.0eV	28.08	932.2 eV	45.09	934.11 eV	26.83

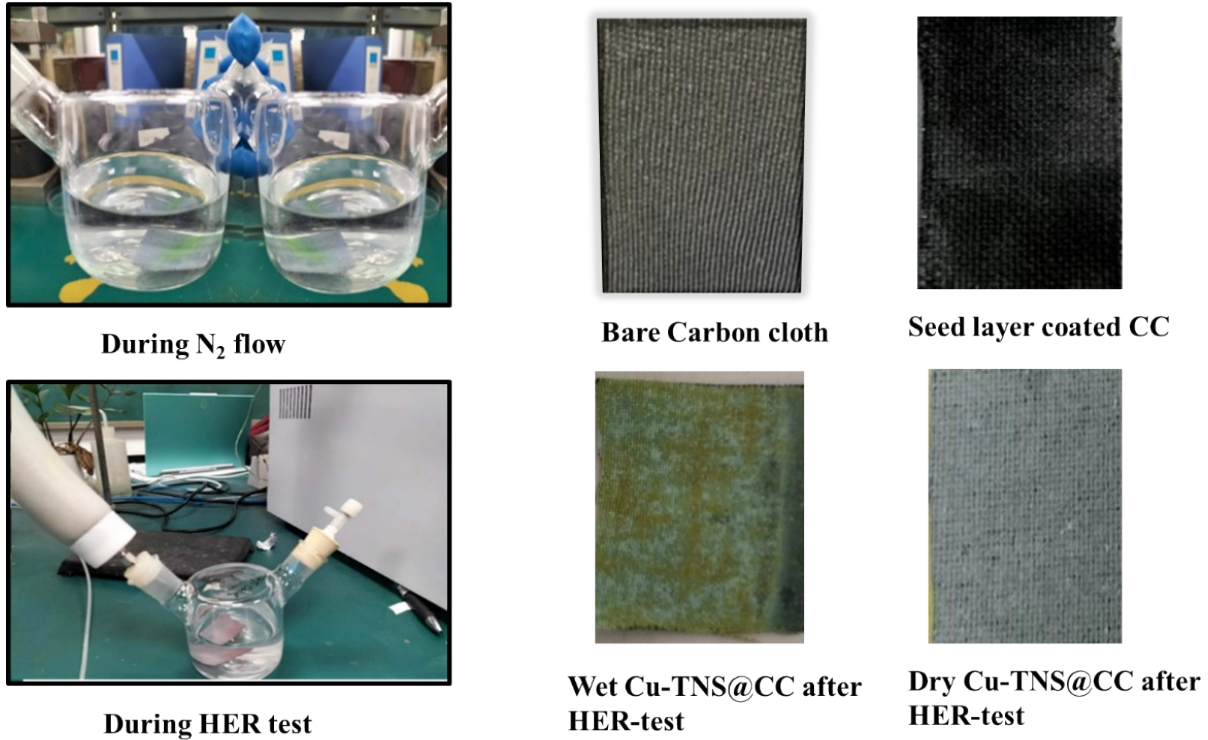


Figure S7: Graphical representation of Cu-TNS@CC at different stage during test.

Table S3: H₂ evolution rate of Cu-TiO₂ using carbon cloth as a substrate

Photocatalyst	Light source	Method	Morphology	Sacrificial reagent	Activity (μmol g ⁻¹ h ⁻¹)	Year	Reference
10%Cu-TNS@CC	300 W Xenon lamp	Hydrothermal	nanosheet	Methanol + water (20%)	1765	2026	This study
9%Cu-TNS@CC	300 W Xenon lamp	Hydrothermal	nanosheet	Methanol + water (20%)	1540	2026	This study
CFcloth @BiOBr/CuO	300 W Xenon lamp	ionic layer adsorption and reaction (SILAR)	nanosheet	Na ₂ S+NaCl +Na ₂ SO ₃	1863	2023	1
TiO ₂ /CuO/Cu	300W Xenon lamp	foaming-assisted electrospinning	Nanofiber	Methanol (100%)	851	2016	2
TiO ₂ NS with Cu@FTO	300WXenon lamp	photo deposition method	Nanosheet	Methanol 60MM	3700	2014	3

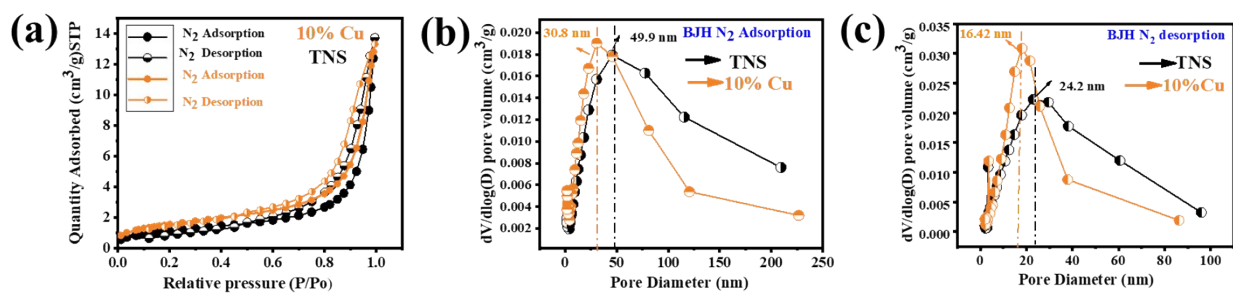


Figure S8: (a) N₂ adsorption-desorption isotherm of Pristine TNS@CC and 10%Cu-TNS@CC, (b-c) BJH pore size distribution of TNS@CC and 10%Cu-TNS@CC nanosheet obtained from N₂ adsorption-desorption analysis.

Table S4: BET surface analysis and pore size distribution.

No.	Synthesized Catalyst	BET surface Area (m ² /g)	Pore Volume (cm ³ /g)	Average pore size
1	TNS@CC	4.15	0.021	19.74
2	10wt%Cu-TNS@CC	5.6	0.020	14.05

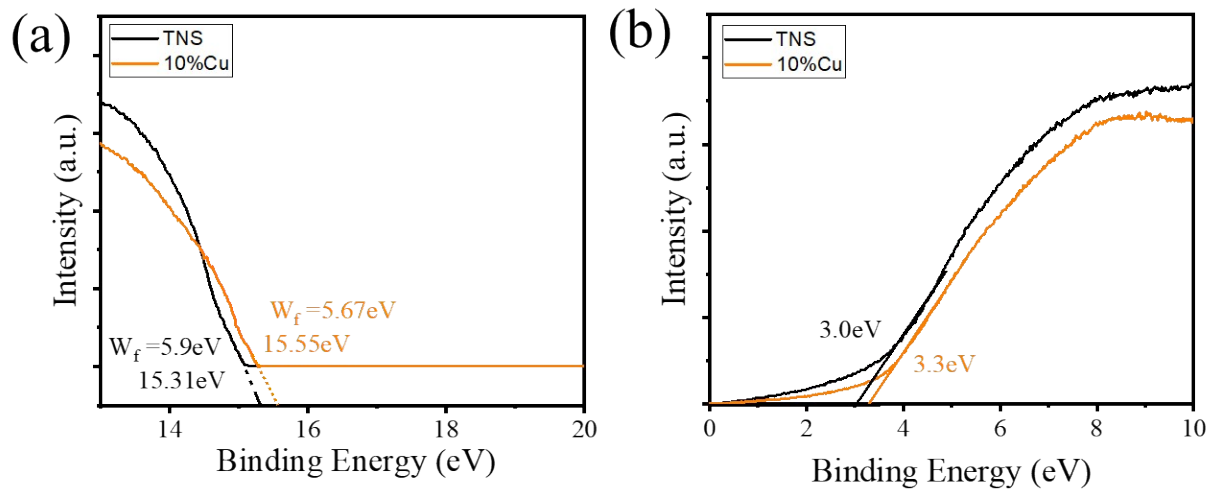


Figure S9: UPS spectrum shows the secondary electron cutoff (a) and valence band region (b) of pristine TiO₂-NS and Cu-doped TiO₂-NS.

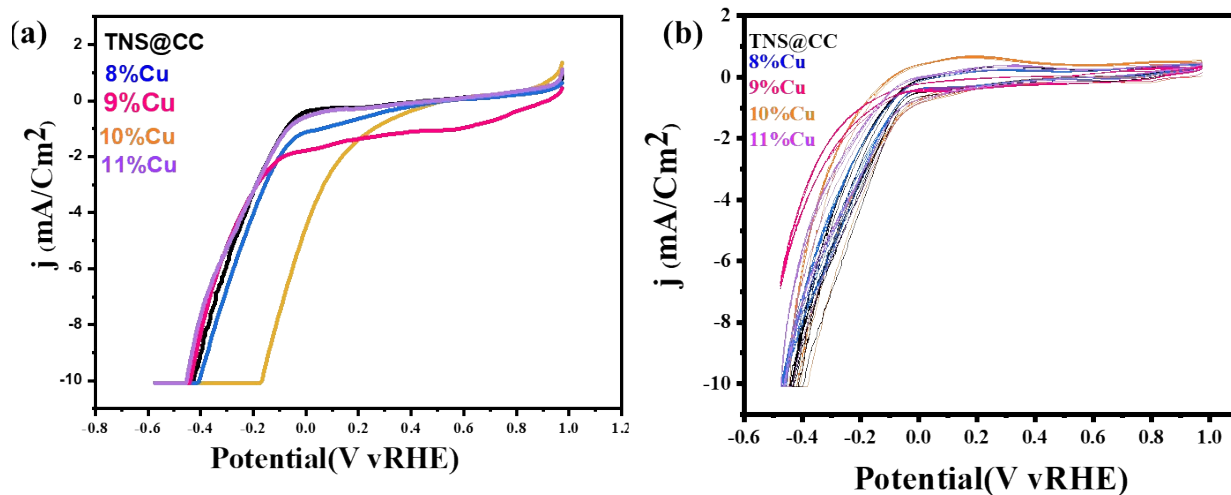


Figure S10: (a) Linear sweep voltammetry (LSV) and (b) Cyclic voltammetry (CV) curves of pristine and 8-11wt% Cu-TNS@CC measured in 1M KOH solution.

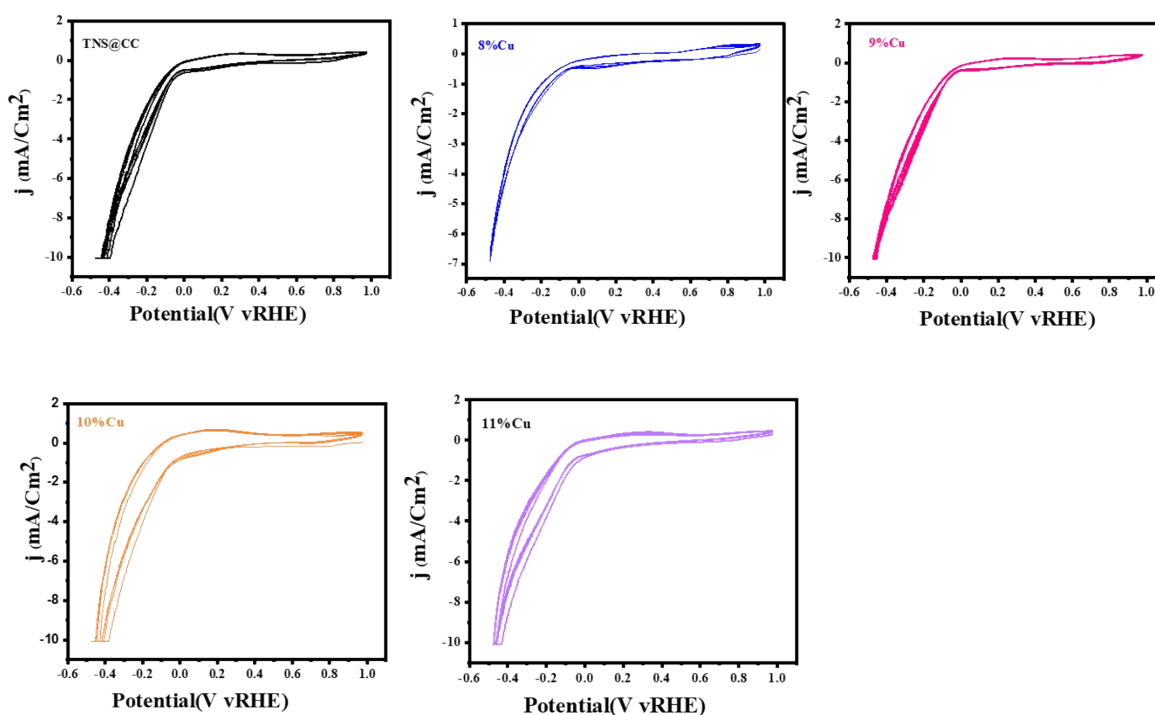


Figure S11: Multiple cycles of cyclic voltammetry (CV) curves of pristine and 8-11wt% Cu-TNS@CC measured in 1M KOH solution.

Electrocatalytic HER Performance of Cu–TNS@CC (Discussion)

The electrocatalytic hydrogen evolution reaction (HER) activity of pristine and Cu-decorated TiO₂ nanosheets supported on carbon cloth (TNS@CC) was systematically evaluated in 1 M KOH using linear sweep voltammetry (LSV) and cyclic voltammetry (CV), as presented in Fig. S10-11.

The LSV curves (Fig. S10a) reveal a pronounced enhancement in HER activity upon Cu incorporation. Compared to pristine TNS@CC, all Cu-modified electrodes exhibit a significant increase in cathodic current density and a positive shift in onset potential by 230mV, indicating improved catalytic efficiency.⁴ Among the investigated compositions, the 10 wt% Cu–TNS@CC sample demonstrates the best performance, delivering the highest current density at a given potential and the lowest overpotential for HER initiation. This suggests that Cu incorporation effectively promotes the electrocatalytic kinetics.⁶ However, a slight decline in performance is observed at 11 wt% Cu loading, which can be attributed to possible agglomeration of Cu species or partial blockage of active sites, thereby limiting electrolyte accessibility and charge transfer.⁵

The enhanced HER activity can be rationalized by considering the role of Cu in modifying the electronic structure of TiO₂. Pristine TiO₂ is inherently limited by poor electrical conductivity; however, Cu decoration introduces conductive pathways that facilitate rapid electron transport. Furthermore, Cu sites are known to optimize the hydrogen adsorption free energy (ΔG_{H^*}), bringing it closer to thermoneutral conditions, which is essential for efficient HER catalysis.⁷ In alkaline media, where water dissociation is a key step, Cu may also accelerate the Volmer step by promoting H₂O adsorption and dissociation, thereby enhancing the overall reaction kinetics.

The CV curves (Fig. S10b and S11) further support these findings by providing insights into the electrochemical surface characteristics of the catalysts. The Cu-modified electrodes exhibit higher current responses and larger enclosed areas compared to pristine TNS@CC, indicating an increased electrochemically active surface area (ECSA). This enhancement suggests that Cu incorporation not only improves intrinsic activity but also exposes more active sites for the HER. The quasi-rectangular and symmetric nature of the CV profiles indicates good electrochemical reversibility and stability of the electrode materials.⁸

A closer inspection of the individual CV profiles (Fig. S10b and S11) shows a consistent trend of increasing current density with Cu loading up to 10 wt%, beyond which the benefit diminishes.⁴ This observation highlights the existence of an optimal Cu concentration, where the balance between active site density, electrical conductivity, and surface accessibility is maximized. Excessive Cu loading may lead to particle aggregation or coverage of catalytically active TiO₂ sites, thereby reducing the overall efficiency.

Overall, the results demonstrate a volcano-type dependence of HER activity on Cu loading, with 10 wt% Cu–TNS@CC emerging as the optimal composition. The superior performance of this electrode can be attributed to the synergistic interplay between Cu and TiO₂, which enhances charge transfer, optimizes hydrogen adsorption energetics, and increases the density of active sites. These findings underscore the effectiveness of transition metal decoration as a strategy to improve the electrocatalytic performance of semiconducting oxide-based HER catalysts in alkaline media.

1. C.-J. Chang, Y.-C. Kao, K.-S. Lin, C.-Y. Chen, C.-W. Kang and T.-H. Yang, *Journal of the Taiwan Institute of Chemical Engineers*, 2023, **149**, 104998.
2. H. Hou, M. Shang, F. Gao, L. Wang, Q. Liu, J. Zheng, Z. Yang and W. Yang, *ACS Applied Materials & Interfaces*, 2016, **8**, 20128-20137.
3. Y. Zou, S.-Z. Kang, X. Li, L. Qin and J. Mu, *International journal of hydrogen energy*, 2014, **39**, 15403-15410.
4. J. N. Hansen, H. Prats, K. K. Toudahl, N. Mørch Secher, K. Chan, J. Kibsgaard and I. Chorkendorff, *ACS Energy Letters*, 2021, **6**, 1175-1180.
5. M. Fazil, S. M. Alshehri, Y. Mao and T. Ahmad, *Langmuir*, 2024, **40**, 4063-4076.
6. Y. Wang, G. Zhang, W. Xu, P. Wan, Z. Lu, Y. Li and X. Sun, *ChemElectroChem*, 2014, **1**, 1138-1144.
7. M. Yousaf, H. Hu, F. Abbas, X. Chen, Y. Wei, M. Sohail and Y. Gao, *Materials Horizons*, 2025, DOI: 10.1039/D5MH01679G.
8. C. Yang, Z. Xiaojun, Z. Qiujuan, M. Xinjia, C. Yan, Y. Weiting and P. Qinhe, *International Journal of Hydrogen Energy*, 2023, **48**, 3759-3767.